Green Chemistry

PAPER

Check for updates

Biodegradable alginate derivatives obtained by eco-friendly ultrasound technology for more sustainable leather tanning†

Ilaria Quaratesi, [a,b] Petre Chipurici, *[c] Vittoria Ferrara,[d,e] Concepció Casas,[f] Anna Bacardit,[f] Noemi Proietti,[g] Carmen Talotta, *[d] Carmine Gaeta, [d] Veronica Iuliano, [d] Immacolata Bruno,[e] Antonio Pauciulo,[e] Rocco Gliubizzi,[e] Ioan Călinescu[c] and Elena Badea *[a,h,i]

This study investigates ten biodegradable re-tanning agents derived from sodium alginate, utilizing various ultrasound technologies and varying key process parameters, including ultrasound frequency, intensity, and treatment duration, at a maintained temperature of 40 °C. The sodium alginate derivatives (SADs) were characterized through viscosimetric analysis, gel permeation chromatography (GPC), proton nuclear magnetic resonance (1H-NMR) spectroscopy, thermogravimetric analysis, and attenuated total reflectance Fourier-transform infrared (ATR-FTIR) spectroscopy. The findings demonstrate that ultrasound primarily facilitates the cleavage of 1–4 linkages within the polymer chains. The thermal stability of SAD-collagen matrices was influenced by the molecular weight and viscosity of the SADs, along with the intrinsic heterogeneity of the collagen matrix. Subsequently, the most effective SAD for the re-tanning process was evaluated at a pilot scale. The leather produced underwent comprehensive characterization through physical–chemical methods (micro-differential scanning calorimetry, unilateral NMR, ATR-FTIR) and standard tests. Notably, the selected SAD fully replaced existing commercial products, such as acrylic resins and synthetic re-tanning agents, resulting in white leather with a natural softness that maintains the technical performance characteristics, such as tear strength, surface durability, grain distention, and colour fastness, required for high-end footwear and leather goods. Additionally, this approach offers enhanced advantages for both human health and the ecosystem by eliminating the need for dyeing processes.

Green foundation

1. This work presents sodium alginate derivatives as non-toxic re-tanning agents, produced using ultrasound (US) technology under mild, solvent-free conditions. The results demonstrate that US improves efficiency, selectivity, and control over sodium alginate depolymerization, resulting in waste-free processing.

2. SADs re-tanning agents from renewable algae provide a sustainable and biodegradable alternative to harmful fossil-based chemicals commonly employed in the tanning process. Their use enhances resource efficiency by promoting waste valorization, diverting approximately 80% of raw materials from harmful incineration or landfill.

3. By integrating algae-based re-tanning agents, the tanning industry can take a meaningful step towards environmental responsibility and circular economy practices. Further research will focus on optimizing US-assisted extraction of alginate from diverse sources and developing value-added derivatives with hydrophobic modifications to enhance the uptake rate of anionic dyes and fatliquors.

[a]National Research & Development Institute for Textiles and Leather, ICPI Research Division, Ion Minulescu Str. 93, 031215 Bucharest, Romania. E-mail: elena.badea@edu.ucv.ro

[b]Alma Mater Studiorum – University of Bologna, CHIMIND, Ue4 via Gobetti, 85, 40129 Bologna, Italy

[c]National University of Science and technology POLITECHNICA Bucharest, Faculty of Chemical Engineering and Biotechnology, Department of Bioresources and Polymer Science, Splaiul Indipendentei 313, 060042 Bucharest, Romania. E-mail: petre.chipurici@gmail.com

[d]Dipartimento di Chimica e Biologia "A. Zambelli", Università di Salerno, Via Giovanni Paolo II 132, I-84084 Fisciano, Salerno, Italy. E-mail: ctalotta@unisa.it

[e]BI-QEM SPECIALTIES SPA, Zona industriale, 84021 Buccino, Salerno, Italy

[f]A3 Leather Innovation Center, Av. Pla de La Massa 8, 08700 Igualada, Barcelona, Spain

[g]Istituto di Scienze del Patrimonio Culturale (ISPC) CNR, Area della Ricerca di Roma 1, 00015 Monterotondo, Roma, Italy

[h]Department of Chemistry, Faculty of Sciences, University of Craiova, Calea Bucuresti Str. 107 I, 200512 Craiova, Romania

[i]The Research Institute of the University of Bucharest, Șoseaua Panduri 90, Sector 5, 050663 Bucharest, Romania

† Electronic supplementary information (ESI) available: Fig. S1: Solid wastes generated by leather manufacturing; Fig. S2: Schematic representation of the ultrasonic devices; Fig. S3: GPC of SA, SAD1-SAD10 and correlation of MW and viscosity of SADs; Fig. S4–S8: ^{1}H NMR spectra of SAD1–SAD10; Fig. S9–S11: ATR-FTIR spectra of SADs and SA; Fig. S12: ATR-FTIR spectra of L1, L2, L3, L4, L5 leathers and of the raw hide; Table S1: Preliminary test on SA to determine the best concentration; Table S2: Mass loss of SA and SADs by TG. Tables S3–S7: Tanning pilot scale process for L1–L5. See DOI: https://doi.org/10.1039/d4gc06571a

Introduction

Leather's enduring popularity stems from its timeless elegance and durability. The global leather industry is a significant economic force, with annual production exceeding 20 billion square feet and a projected market growth from USD 282.7 billion in 2024 to USD 552.9 billion by 2033.[1] Developing countries like Brazil, India, and China are major exporters due to lower labour and production costs, with China leading globally. Europe, while a large consumer, focuses on high-end production through R&D and skilled artisans.[2] Despite its economic importance, leather tanning is environmentally damaging, generating substantial solid and liquid waste. This has increased the focus on sustainability and eco-efficiency. A significant portion of raw materials, around 80%, becomes solid waste. Of the total amount of solid waste generated by leather manufacturing in the main world areas (Fig. S1†), more than 30% is chemically treated proteinaceous waste that persists in the environment and has a significant impact on human health, marine ecosystems, soil, and groundwater.[1–6]

The substitution of chromium and other metal salts with not harmful synthetic tannins (syntans) and natural vegetable tannins promises to tackle the toxic chemicals used in leather production.[3] However, due to the long supremacy of chromium salts in leather tanning, most of the additives used today, including the re-tanning agents (*i.e.* derivatives of phenol, urea, and melamine–formaldehyde and acrylic resins) have been designed for chromium salt tanning technology[4] and cannot be used *for wet white* tanning (*i.e.*, tanning with syntans) or vegetable tanning.[5–7] The re-tanning process is pivotal in determining the quality of leather. In fact, in almost all cases, the leather's initial tanning (also known as primary tanning) is insufficient to maintain the desired properties specified by the customer. It is therefore re-tanning to adjust suppleness, fullness, dyeability, light fastness, and grain stability.[7,8] Recent advancements include the development of polyurethane-based re-tanning agents incorporating hexamethylene diisocyanate, which exhibit antimicrobial properties and enhance leather's mechanical strength.[7] Additionally, melamine ethoxylates synthesized from epoxides present a potential eco-friendly alternative to traditional formaldehyde-based melamine urea re-tanning agents, incorporating renewable materials for sustainability.[8] Novel amphoteric acrylic polymers produced *via* the Mannich reaction show improved dye uptake and assistant-dyeing capabilities over conventional anionic agents.[9] Several formaldehyde-free feel modifiers and fillers have been explored. For instance, a chitosan modified bovine hair keratin-based auxiliary was reported to improve mechanical properties of shoe upper leather.[10] Biodegradable re-tanning agents developed using pretreated raw trimming wastes enhanced leather fullness.[11] Graft copolymers obtained from fleshing hydrolysate with methacrylic acid,[12] as well as from alkaline keratin hydrolysate[13] were applied as re-tanning agent for enhancing organoleptic properties and mechanical strength of leathers. Quimser company has launched commercial bio-based re-tanning agents (SERTAN RN-S, SERTAN PR,

and SERTAN RD) from natural polymers, which they claim enhance leather's adhesion, elasticity, and fiber compactness as eco-friendly alternatives to conventional resins.[14] Algae-derived alginate, one of the most abundant polysaccharides in the world, constituting up to 40% of the dry matter in seaweed, has been investigated as a novel, eco-friendly re-tanning agent. In 2022, the European Commission launched the Communication 'Towards a strong and sustainable EU algae sector', a pioneering initiative to unlock the potential of algae in the European Union based on 23 actions to create opportunities for the industry to help it grow into a robust, sustainable and regenerative sector capable of meeting the growing EU demand.[15] Notably, in Romania, more than 10 tons of algae are lost through disuse, ending up in landfills.[16] However, earlier research shows that the sodium alginate (SA) and its derivatives' high viscosity severely limits their use in tanning.[17,18,20,21] While various chemical modifications like oxidation, esterification and graft polymerisation have been employed for sodium alginate, periodate oxidation has been primarily investigated for collagen crosslinking and leather tanning at a lab scale[19–21] Some of us showed that, from the laboratory to industrial pilot level, oxidized alginate combined with nano-hydroxyapatite improves flame retardancy and thermal stability of leather.[22,23] Since ultrasonic treatment has been demonstrated to be effective in reducing alginates' viscosity and molecular weight, its use could offer a potentially greener and more easily implementable solution for the leather industry.[24–26]

In this study, the ultrasound technology has been utilized to process alginate into a re-tanning agent without harsh chemicals, aligning with circular economy principles.[27] This approach also addresses the limitations of periodate oxidation, which has safety and import restrictions.[28–30] Diverse ultrasonic equipment and process parameters—such as frequency, intensity, and treatment duration—were used to generate several sodium alginate derivatives (SADs). Subsequently, we characterized these derivatives and evaluated their potential as non-toxic and biodegradable re-tanning agents for wet-white and vegetable tanning. The development of non-toxic and biodegradable re-tanning agents supports the revalorization of leather solid waste and improves the perception of leather's sustainability. This research is based on the alignment of scientific knowledge, environmental responsibility, and the growing consumer preference for sustainable goods.

Results and discussion

Ultrasound-assisted preparation of sodium alginate derivatives (SADs)

It is well known that the use of different types of ultrasonic transducers (*i.e.* magnetostrictive and piezoelectric) may result in different end products.[31] Piezoelectric transducers are characterised by a small tip from which high-intensity ultrasound is radiated converting alternating electrical energy directly into mechanical energy, while magnetostrictive trans-

ducers utilize the magnetostrictive property of a material to convert the energy in a magnetic field into mechanical energy.[32,33] Three distinct types of equipment (Fig. S2†) were utilized in the study, two of which employed piezoelectric transducers—one operating at a frequency of 20 kHz and the other a multifrequency model functioning at medium to high frequencies: 580, 864, and 1146 kHz. The third piece of equipment utilized two magnetostrictive transducers operating at 16 kHz and 20 kHz frequencies. This setup underscored the significance of both frequency and power density at the surface of the transducers.

The Vibracel equipment features a probe with a diameter of 13 mm; with a power output of 60 W, it achieves a power density of 45.23 W cm^{-2}. In contrast, the MU equipment is equipped with a 50 mm diameter transducer that operates at 50 W, resulting in a power density of 2.54 W cm^{-2}. Meanwhile, the DFR equipment, which consists of two magnetostrictive transducers, each with a diameter of 10 cm, also uses 50 W of power per transducer, yielding a lower power density of just 0.64 W cm^{-2}.[34]

Additionally, the reactors associated with these three pieces of equipment vary significantly in volume, ranging from 20 mL for the MU equipment to 600 mL for the DFR setup. Consequently, a broad spectrum of ultrasound treatment conditions was explored to determine the most efficient methods for achieving optimal solvent-assisted extractions (SADs). Ten tests were conducted at 40 °C to compare the effects of ultrasonic energy generation mechanisms, reactor configuration, and different frequencies and sonication times, on SA dispersions of 2% w/w (Table 1).

An important consideration when using ultrasound is the temperature of the solvent. Higher temperatures can help break down solute–matrix interactions, such as van der Waals forces, hydrogen bonding, and dipole attractions. However, lower temperatures facilitate a better cavitation phenomenon. As the solvent temperature rises, its vapor pressure also increases, leading to more solvent vapor filling the cavitation bubbles, which tend to collapse less violently.[33,35,36] For this reason, a temperature of 40 °C was selected for all experiments. This choice balances the benefits of cavitation with the

consideration that 40 °C requires less energy, making it more efficient for scaling up the process to an industrial level. The effectiveness of US treatment is greatly affected by the viscosity of the medium, as a high-viscosity medium impedes the spread of ultrasound waves and diminishes cavitation effects.[37] A preliminary study was therefore conducted to determine the optimal concentration of the SA water dispersion (see Table S1†).

Characterization of sodium alginate derivatives (SADs)

Molecular weight distribution by viscosity and GPC analyses. Ultrasounds modify alginate by reducing its molecular weight through polymer chain scission, primarily caused by the hydrodynamic forces generated during the sonication process.[38,39] The US-induced change in molecular weight distribution of the ten SADs was investigated using GPC analysis. Furthermore, the final viscosity of SADs solutions was determined as viscosity stands out as a critical parameter for the suitability of a product in the tanning process.[40,41] As illustrated in Table 2, which presents the molecular weights, polydispersity index (PDI), and viscosities of the sodium alginate derivatives (SADs), the ultrasonic horn transducer produces a very low viscosity product (SAD1, SAD2, and SAD3). This transducer has a small active cavitation zone but a larger radiating surface, resulting in highly concentrated energy.[42–44] Conversely, the DFR reactor reduces the viscosity of the sodium alginate solution, albeit to a lesser extent (SAD4, SAD5, SAD6, and SAD7).[45]

The US frequency had the most significant impact on viscosity, as shown in Table 2. Specifically, medium to high frequencies led to an increase in viscosity compared to sodium alginate (SA) (i.e., SAD8, SAD9 and SAD10). This effect can be attributed to the differing physical and chemical interactions generated by varying frequencies: low-frequency ultrasonics produce strong physical effects,[46] while medium to high frequencies induce intense chemical reactions with minimal physical impact. In fact, cavitation bubbles formed at medium to high frequencies are considerably smaller and more prone to resonance rather than collapse, in contrast to those created at lower frequencies.[31,43] In our case, this results in a lower

Table 1 Sodium alginate derivatives (SADs) obtained using different transducers and process parameters

Sample name	Transducer	Frequency (kHz)	US power (W)	Sample volume (mL)	Sonication time (min)	Total time (min)	Air flow (L h^{-1})
SAD1	VCX 750	20	60	40	30	60	10
SAD2	VCX 750	20	60	40	60	120	10
SAD3	VCX 750	20	60	40	90	180	10
SAD4	DFR	20 + 16	100	600	30	30	400
SAD5	DFR	20 + 16	100	600	60	60	400
SAD6	DFR	20 + 16	100	600	90	90	400
SAD7	DFR	20 + 16	100	600	120	120	400
SAD8	MU	580	50	20	60	60	4.5
SAD9	MU	864	50	20	60	60	4.5
SAD10	MU	1146	50	20	60	60	4.5

S.A. 2% w/w, $T \approx 40$ °C; VCX 750 – Sonic Vibracell VCX 750 ultrasonic processor; DFR – closed loop dual-frequency reactor (DFR) with two bath-type transducers (16 kHz and 20 kHz); MU – Meinhardt ultrasonics multifrequency transducer.

Table 2 Molecular weights, polydispersity index (PDI), and viscosity of the ten SADs compared to that of the initial SA 2% solution

Sample	Viscosity (cP)	Retention time (min)	M_p (Da)	M_w (Da)	M_n (Da)	PI
SA 2%	3950	24.000	—	>739 000	—	—
SAD1	60	32.763	506 816	436 929	368 510	1.19
SAD2	23.5	34.980	250 532	266 749	216 057	1.23
SAD3	14	35.467	214 616	219 638	190 818	1.15
SAD4	2237	30.633	999 534	965 905	817 686	1.18
SAD5	1097	31.246	821 635	754 793	584 542	1.29
SAD6	695.6	31.321	802 234	717 871	604 515	1.19
SAD7	579.1	32.095	626 808	684 008	562 099	1.22
SAD8	7038	30.532	1 032 743	1 102 974	965 574	1.14
SAD9	5458	30.265	1 124 826	987 754	805 929	1.23
SAD10	5840	30.066	1 199 104	1 067 581	899 282	1.19

degree of depolymerisation, as the mechanical action is reduced. Furthermore, as the chemical effect is predominant, more chemically active radicals may be formed, leading to re-polymerisation,[47,48] and viscosity increase, as for the SAD8, SAD9 and SAD10. According to data shown in Table 2 and GPC profiles (Fig. S2†) of the ten SADs, the viscosity reduction can be effectively achieved by using a lower ultrasonic frequency, higher amplitude, and longer sonication time. In fact, SAD1, SAD2 and SAD3 had the greatest right shift relative to SA (Fig. S2†), confirming a significant reduction in the polymer's molecular mass and the highest degree of depolymerization. On the contrary, SAD 8, SAD 9 and SAD 10, obtained at mid-high US frequencies, had a shorter flow time, resulting in higher molecular weight distributions. Nonetheless, the poly-dispersity values (Table 2) are all in the range of (1.1–1.3), indicating that all SAD solutions are homogeneous and bond cleavage was the main phenomenon that occurred.

The polydispersity index (PDI), calculated as the ratio of the weight-average molecular weight (M_w) to the number-average molecular weight (M_n), measures the breadth of the molecular weight distribution in polymers.[49] The higher the PDI the broader the molecular weight distribution. The variations in the dispersity of the sodium alginate derivatives (SADs),

ranging from 1.14 (SAD8) to 1.29 (SAD4), are modest, suggesting that ultrasonic treatment depolymerizes alginate into homogeneous oligo-alginates with narrower molecular weight distributions. These findings are consistent with the results from the NMR and ATR-FTIR analyses, which indicate that cleavage of the β-1,4 or α-1,4 bonds is the most likely occurrence. Fig. 1 depicts the expected cleavages within the alginate polymeric chains during the ultrasonic treatment.

^{1}H NMR study of SADs. The distribution of guluronate (G) and mannuronate (M) blocks in alginate molecules is influenced by the type of seaweed, as well as the age and specific section of the algae from which the alginate is harvested.[50,51] As it is known, long sequences of guluronate cause alginate chains to become stiffer, leading to the formation of rigid and brittle gels. In contrast, a higher proportion of mannuronate contributes to the creation of softer and more elastic gels. However, in the presence of hybrid MG blocks, alginate shrinks and becomes more flexible.[51] For a re-tanning agent to be effective, the leather needs to be soft and pliable; therefore, a higher ratio of M-blocks is preferred. Following a standard protocol previously described in the literature,[52,53] the M/G ratio in sodium alginate derivatives (SADs) was analysed using ^{1}H NMR analysis (Table 3).
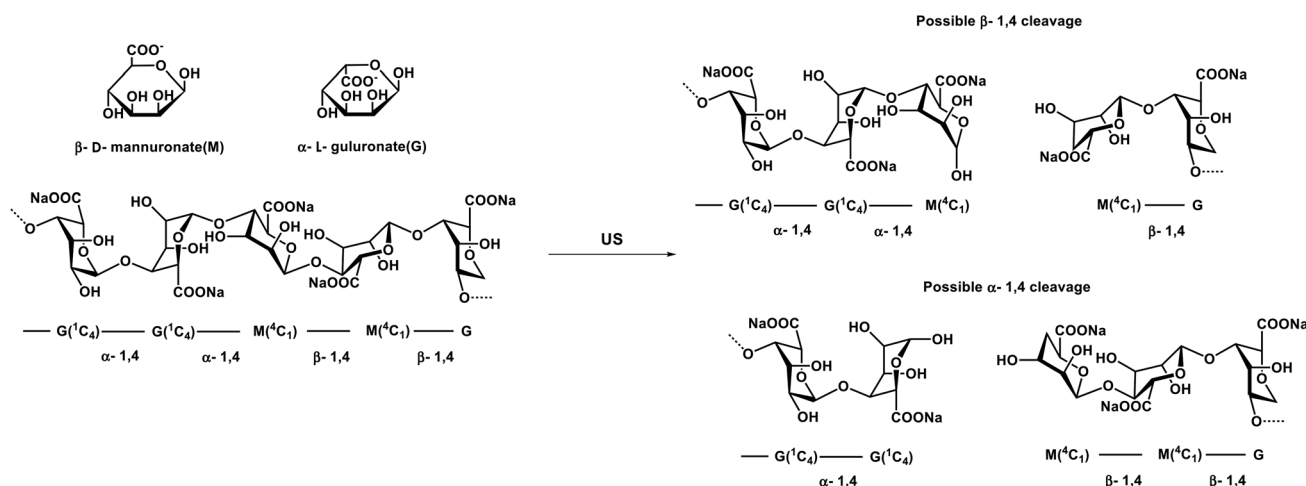

Fig. 1 Possible cleavages due to ultrasonic treatment.

Table 3 Mannuronate (M) and guluronate (G) ratio for the obtained SADs

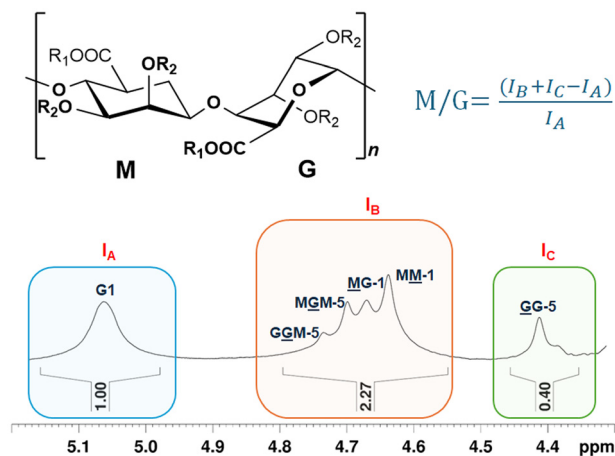| Sample	SAD1	SAD2	SAD3	SAD4	SAD5	SAD6	SAD7	SAD8	SAD9	SAD10
M/G ratio	1.56	1.63	1.79	1.75	1.68	1.68	1.26	1.54	1.49	1.42

Fig. 2 A relevant portion of the ^1H NMR spectrum (600 MHz, 353 K, D$_2$O) of SAD5 displays the signals attributed to the following: the anomeric hydrogen atom of glucuronic acid (G1); the H-5 atom of the core guluronic acid residue in the GGM triad (GGM-5); the H-5 atom of the MGM triad (MGM-5); and the anomeric hydrogen atom of the mannuronic acid residue (MM-1).

Fig. 2 presents a significant portion of the ^1H NMR spectrum (600 MHz, 353 K, D$_2$O) obtained for SAD5, where a prominent signal at 5.02 ppm is attributed to the anomeric hydrogen atom of glucuronic acid (G-1). The signal observed at 4.72 ppm is attributable to the H-5 atom of the core guluronic acid residue in the GGM triad (GGM-5), while the signal at 4.69 ppm is associated with the H-5 atom of the MGM triad (MGM-5). Additionally, the NMR signal at 4.66 ppm has been assigned to the anomeric hydrogen atom of the mannuronic acid residue (MM-1).

The M/G ratios were calculated by integrating specific spectral regions of the ^1H NMR spectrum (Fig. 2): region A (4.96–5.18 ppm), region B (4.57–4.82 ppm), and region C (4.38–4.55 ppm). The corresponding integrals, I_A, I_B, and I_C, were then used in Jensen's equation, reported in Fig. 1, to calculate the M/G ratio (Table 3) showing an excess of M units across all derivatives.

ATR-FTIR characterization of SADs. The ATR-FTIR spectra of sodium alginate (SA) and sodium alginate derivatives (SADs) were recorded and compared (Fig. S9–S11†). Both the sodium alginate (SA) and sodium alginate derivative (SAD) spectra display significant absorption bands corresponding to OH stretching vibrations involved in intramolecular and intermolecular H-bonding (3260 and 2934 cm^{-1}), asymmetric and symmetric stretching vibrations of carboxylate (COO$^-$) (1597 and 1402 cm^{-1}), and glycosidic bonds C–O–C stretching vibrations (1078 and 1024 cm^{-1}).[21,54–56] In addition, the

anomeric region (950–750 cm^{-1}) is assigned to the vibration of uronic acid residues, *i.e.*, C–O stretching vibration of uronic acids with contributions from C–C–H and C–O–H deformation (946 cm^{-1}) and deformation vibration of β-C1–H mannuronic acid residue (878 cm^{-1}).[57,58] The band at 814 cm^{-1} are attributable to the stretching vibrations of C–H bonds and the band at 616 cm^{-1} to the C–C–C ring in-plane bending.[59,60] As illustrated in Fig. S9–S11,† no significant changes were observed following ultrasonic processing, as expected. The SA characteristic functional groups, such as hydroxyl, carboxylate, and glycosidic bonds, remain unchanged (no significant shifts or deformations of the bands are observed), resulting in similar spectral features despite molecular mass and viscosity differences. Both SA depolymerization and aggregation processes induced by US primarily reduce or increase molecular weight, as indicated in Table 2, without breaking characteristic functional groups or bonds. The only noticeable difference among the three groups is the intensity of the bands, specifically, the intensity of the hydroxyl band at 3260 cm^{-1}, which increases from the SAD8–SAD10 group, with the highest viscosity, to the SAD1–SAD3 group, with the lowest viscosity. This might be attributed to the formation of new hydroxyl groups through the glycosidic bonds' cleavage.

Thermal degradation of SADs. Thermogravimetry is a technique that provides information about moisture and ash content in a straightforward and rapid manner. The TG curves reported in Fig. 3 illustrate the mass loss of SAD2 compared to SA.

According to the literature, sodium alginate exhibits three thermal events (mass loss) in the intervals (25–200) °C, (200–300) °C and (300–800) °C.[61] The first event is endothermic and corresponds to dehydration (residual moisture of the polysaccharide and water bound more internally to the algi-
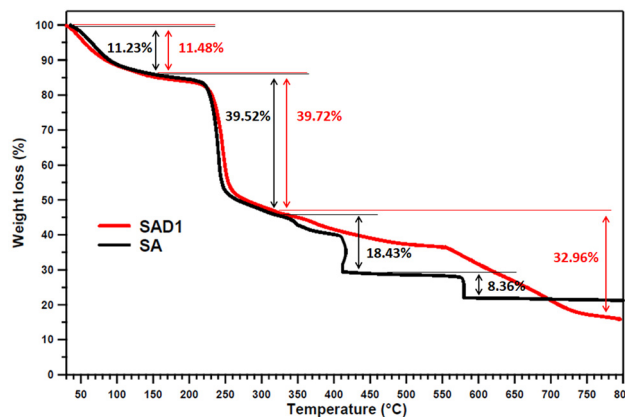

Fig. 3 TG curves of SAD1 and SA illustrate the three stages of thermal degradation and percentage of weight loss *vs.* temperature.

nate structure), while the second and third events are exothermic, and are associated with the degradation of anhydrous sodium alginate and formation of sodium carbonate, followed by its decomposition to sodium oxide and carbon dioxide release. A similar behaviour was found for all SADs (Table S1†), confirming that the main phenomenon occurring while using US is polymer chain cleavage.

Characterization of collagen-SADs matrices: laboratory scale

Differential scanning calorimetry (DSC) is used to analyse protein stability by monitoring thermal properties during heating. It measures excess heat capacity as temperature changes, allowing for the evaluation of protein unfolding or denaturation. DSC uniquely estimates the enthalpy of denaturation making it essential for protein engineering, biopharmaceutical formulation, and studying ancient protein-based materials.[62–67] Recently, we utilized micro-DSC for the first time to assess newly synthesized tanning agents' properties and their ability to penetrate the leather structure uniformly and bond with collagen.[22,68] Through DSC, we evaluate this penetration and leather's thermal stability by examining calorimetric peak characteristics.[82] The denaturation curve reveals thermodynamic properties, while thermogram deconvolution provides insights into collagen populations with distinct thermal stability. Fig. 4 compares the denaturation peaks of calf hides treated with the newly obtained SADs to raw hide, while their denaturation parameters are listed in Table 4.

Experimental results demonstrate that the interaction between collagen and SADs improves the matrix's hydrothermal stability. The denaturation temperature (T_{max}) increased by more than 5 °C for all samples, except for SAD3 and SAD10, and the denaturation enthalpy increased by more than 50%. However, one or two shoulders occur on the denaturation peaks at temperatures higher than T_{max}, indicating a certain heterogeneity in thermal stability. This might be ascribed to the structural heterogeneity of the collagen-SAD matrix alone, given that the tanning conditions were identical for all collagen-SAD matrices. SADs can interact with collagen primarily through electrostatic interactions and hydrogen bonding, but the nature of these interactions is less rigid than the covalent bonding that vegetable- or aldehyde-based tannins might induce.[22] Both the density and spatial distribution of these bonds influence the thermal stability of the SAD-collagen matrices. The molecular weight and degree of polymerization of SADs can affect how tightly they bind to the collagen fibres. Medium molecular weight SADs are expected to form more rigid, stable networks, while both lower and higher molecular weight SADs may not crosslink as effectively, leading to regions of weaker thermal stability. In addition, the collagen matrix itself is not homogenous, leading to microregions with distinct thermal stability. Although the chemical composition and structural organisation of collagen at the supramolecular level are the same for different types and different anatomical areas of the hide, its morphology (*i.e.*, the arrangement, density, and wave angle) is intrinsically heterogeneous throughout the collagen matrix. Depending on the
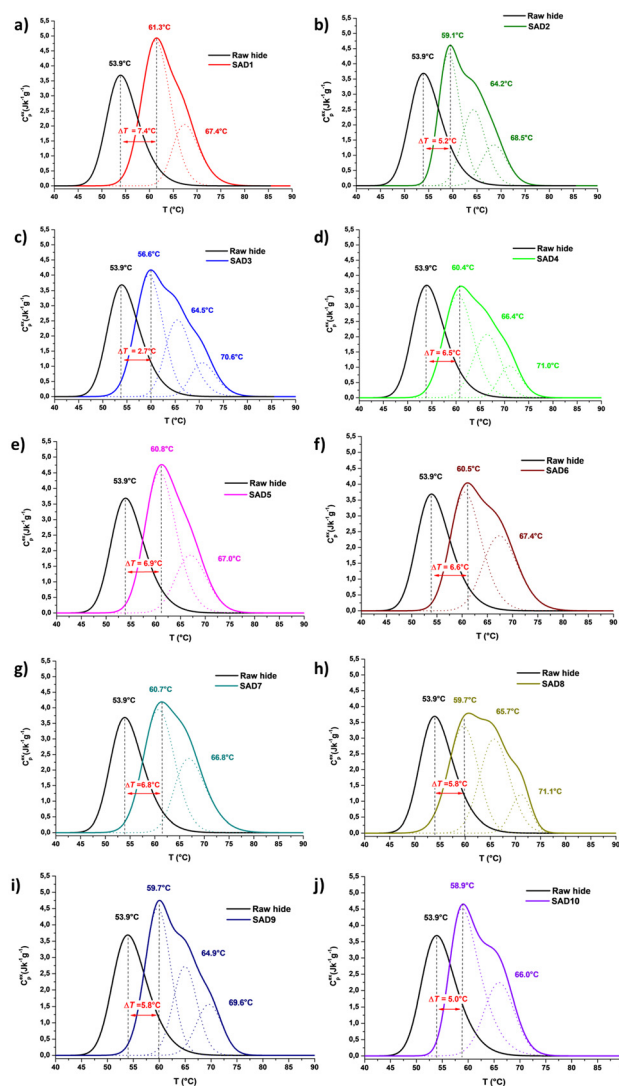

Fig. 4 Thermal denaturation peaks obtained by micro-DSC in excess water, at a heating rate of 0.5 °C min^{-1}, for raw hide (black) and hides treated with (a) SAD1, (b) SAD2, (c) SAD3, (d) SAD4, (e) SAD5, (f) SAD6, (g) SAD7, (h) SAD8, (i) SAD9 and (j) SAD10. For multi-component denaturation peaks, deconvolution into component peaks was applied.

animal species and anatomical part of the hide, pores can range from micropores (diameter < 100 nm) and mesopores (100 nm < diameter < 500 nm) to macropores (diameter > 1 μm).[69,70] Thus, the potential for penetration and interaction with collagen fibers of SAD particles, which depend on their average size distribution and viscosity, can lead to regions with more abundant and stable interactions, more resistant to thermal denaturation, while regions with incomplete or poorly formed interactions will be more susceptible to thermal degradation. For instance, the most homogenous tanning effect is obtained for SAD1, SAD5 and SAD10, yet the increase of denaturation temperature ΔT (*i.e.*, 7.4 °C > 6.9 °C > 5.0 °C) shows clear dependence on viscosity and SAD's size. As expected, SAD3 (lowest viscosity), SAD8, SAD9 and SAD10 (highest viscosity) showed the lowest ability to increase the thermal stabi-

Table 4 Micro-DSC parameters of thermal denaturation of collagen-SAD matrices: onset temperature (T_{onset}), denaturation temperature (T_{max}), peak half-width ($\Delta T_{1/2}$), and denaturation enthalpy (ΔH). The same parameters are reported for the not-treated hide for comparison. ΔT reflects the increase of T_{max} as a result of the interaction between collagen and each SAD

Sample	T_{onset} (°C)	$T_{max\ i}{}^a$ (°C)	ΔT^b (°C)	$\Delta T_{1/2}$ (°C)	$\sum \Delta H_i{}^a$ (J g^{-1})	% $\Delta H_i{}^a$
Raw hide	47.7	$T = 53.9$	—	7.8	31.6	$\Delta H = 100$
SAD1	54.3	$T_1 = 61.3$	7.4	10.2	51.7	$\Delta H_1 = 71.3$
		$T_2 = 67.4$				$\Delta H_2 = 28.6$
SAD2	54.3	$T_1 = 59.1$	5.2	10.9	49.3	$\Delta H_1 = 50.2$
		$T_2 = 64.2$				$\Delta H_2 = 31.6$
		$T_3 = 68.5$				$\Delta H_3 = 18.2$
SAD3	53.8	$T_1 = 56.6$	2.7	13.1	54.2	$\Delta H_1 = 53.4$
		$T_2 = 64.5$				$\Delta H_2 = 32.9$
		$T_3 = 70.6$				$\Delta H_3 = 13.7$
SAD4	54.8	$T_1 = 60.4$	6.5	13.2	47.0	$\Delta H_1 = 55.6$
		$T_2 = 66.4$				$\Delta H_2 = 31.4$
		$T_3 = 71.0$				$\Delta H_3 = 13.0$
SAD5	54.3	$T_1 = 60.8$	6.9	10.4	51.0	$\Delta H_1 = 70.9$
		$T_2 = 67.0$				$\Delta H_2 = 29.1$
SAD6	54.3	$T_1 = 60.5$	6.6	12.5	50.2	$\Delta H_1 = 58.4$
		$T_2 = 67.4$				$\Delta H_2 = 41.5$
SAD7	54.1	$T_1 = 60.7$	6.8	11.7	50.7	$\Delta H_1 = 61.9$
		$T_2 = 66.8$				$\Delta H_2 = 38.1$
SAD8	53.4	$T_1 = 59.7$	5.8	14.7	53.4	$\Delta H_1 = 47.5$
		$T_2 = 65.7$				$\Delta H_2 = 41.4$
		$T_3 = 71.1$				$\Delta H_3 = 11.1$
SAD9	53.9	$T_1 = 59.7$	5.8	11.6	54.1	$\Delta H_1 = 52.5$
		$T_2 = 64.9$				$\Delta H_2 = 29.3$
		$T_3 = 69.7$				$\Delta H_3 = 18.2$
SAD10	53.5	$T_1 = 58.9$	5.0	11.4	50.9	$\Delta H_1 = 67.1$
		$T_2 = 66.0$				$\Delta H_2 = 32.9$

^{a} i = 1–3 represents the index of collagen population with distinct hydrothermal stability. ^{b} Represent the Δ between the collagen population of raw hide and the maximum peak of collagen population of the hide treated with the corresponding SAD.

lity of rawhide ($T_1 < 60$ °C). This could be related to the reduction of SAD interaction sites below a critical number caused by either advanced depolymerization or aggregation.

Considering the properties of the ten sodium alginate derivatives (SADs) and their scalability potential within the ultrasonic process, we selected SAD5 for evaluation in wet-white/mixed wet-white and vegetable re-tanning procedures at the pilot level. Magnetostrictive transducers (used to obtain SAD5) can be used for long periods without altering their performance, and the "closed loop" assembly can be easily scaled up. The flow type is the preferred design for continuous, large-scale processing, as it facilitates improved control over reaction conditions, enhances heat and mass transfer, and provides greater operational flexibility.[39]

Pilot scale tests: characterisation of leather samples by micro-DSC, ATR-FTIR, NMR MOUSE and test methods for industry

To minimize the reliance on synthetic re-tanning agents derived from fossil sources and to investigate the synergistic effects of SAD5 in conjunction with a vegetable tannin, five experimental tests were conducted. In these tests, SAD5 sequentially replaced commercial chemical agents used in the re-tanning phase, as detailed in Table 5. Tara tannin (*Caesalpinia spinosa*) was utilized in these experiments. The specific re-tanning formulations are outlined in Tables S2–S6.†

It is important to note that wet-white leathers are produced through the combination of synthetic and vegetable tannins,

Table 5 Re-tanning agents' combinations in the wet-white re-tanning tests performed at pilot scale level

Leather specimen	Commercial synthetic agent (%)	Commercial acrylic resin (%)	Tara (%)	SAD5 (%)
L1	20	2	10	0
L2	20	0	10	2
L3	0	2	10	20
L4	0	0	10	22
L5	0	0	0	32

enabling a chromium-free operation using the same equipment employed in chrome tanning processes.

The SAD5 efficacy as a re-tanning agent was evaluated by comparing the thermal stability of the specimens L2–L5 with that of L1 specimen. Thermal denaturation peaks (Fig. 4) and their related parameters (Table 6) indicate that L2 behaves similar to L1 (the two denaturation peaks overlap), while L3, L4 and undergone partial de-tanning: the area of peak with the highest T_{max} decrease and a peak with a lower T_{max} occur and progressively increase. L2's thermal stability is maintained since the synthetic re-tanning agent remains present in the same quantity, while a minor amount of SAD5 (*i.e.*, 2%) was added. The decrease of T_{max} for L3–L5 was expected given the ability of SADs to increase the hide thermal stability up to 71 °C, as shown in the previous paragraph (Table 4). Interestingly, this progressive decrease is accompanied by an

Table 6 Thermal denaturation parameters: onset temperature (T_{onset}), denaturation temperature (T_{max}), peak half-width (ΔT_{12}) and denaturation enthalpy (ΔH) for L1–L5 leather specimens

| Test's name	T_{onset} (°C)	$T_{max\ i}{}^{a}$ (°C)	$\Delta T_{1/2}$ (°C)	$\sum \Delta H_i{}^{a}$ (J g^{-1})	% $\Delta H_i{}^{a}$
L1	75.3	T_1 = 79.1	3.69	14.6	ΔH_1 = 100
L2	75.5	T_1 = 78.7	3.59	15.3	ΔH_1 = 100
L3	70.5	T_1 = 76.8	5.46	18.9	ΔH_1 = 24.2
		T_2 = 73.1			ΔH_2 = 75.8
L4	69.8	T_1 = 78.2	4.73	18.1	ΔH_1 = 17.6
		T_2 = 72.6			ΔH_2 = 82.4
L5	67.4	T_2 = 75.1	3.76	20.6	ΔH_2 = 11.6
		T_3 = 70.7			ΔH_3 = 88.4

^{a} i = 1–2 represents the index of collagen population with distinct hydrothermal stability.

increase of the denaturation enthalpy, which reaches the maximum value for L5 specimen. We could therefore assume an increase of bond density within the collagen matrix due to the interaction with SAD5 as its concentration increases from 20% to 22% and 32%. We can state that the three groups of peaks identified by micro-DSC correspond to the following collagen populations: collagen-synthetic re-tanning agent, collagen-tara and collagen-SAD5, in descending order of thermal stability (Fig. 5).

Relaxometric characterization (NMR MOUSE) of leather specimens was carried out to complete the calorimetric results and help us understand which of the 4 combinations containing SAD5 are effective and could be transferred into practice. The values of proton-spin lattice (or longitudinal) T_1 relaxation time and components of the spin–spin (or transverse) T_2 relaxation time are listed in Table 7 and Fig. 6.

As previously reported by Badea *et al.*,[71] the longitudinal T_1 is more sensitive to the type of tannin (*i.e.*, the type of collagen-tannin interaction), whereas the transverse relaxation
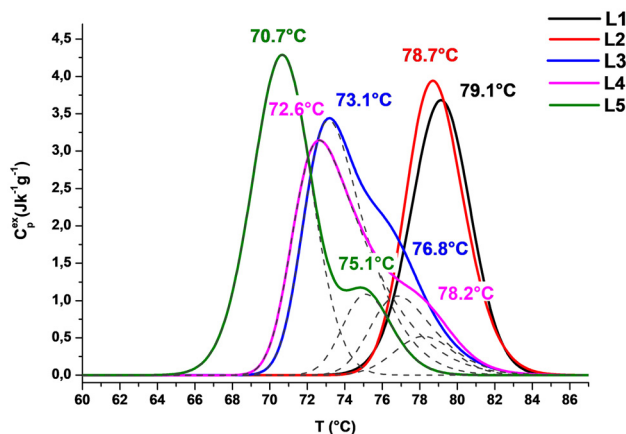
Fig. 5 Thermal denaturation peaks of L1 (black), L2 (red), L3 (blue), L4 (pink) and L5 (green) specimens measured by micro-DSC in excess water, at 0.5 °C·min^{-1}.
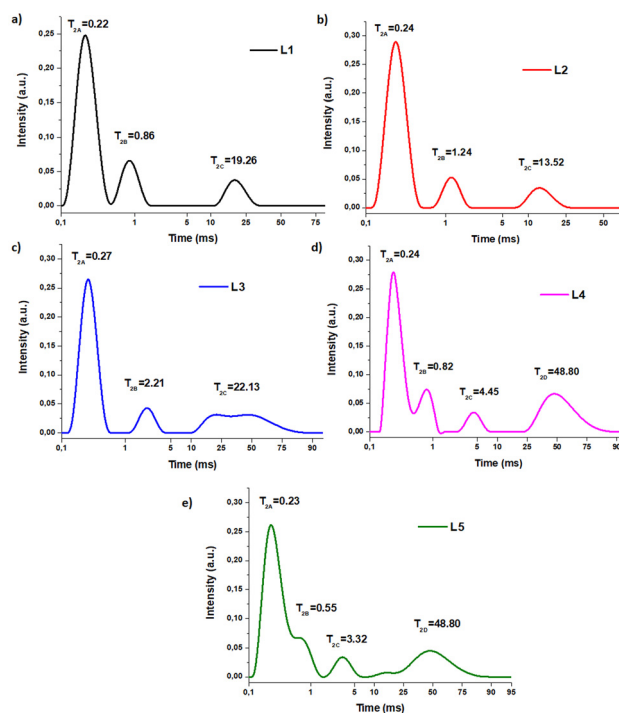
Fig. 6 Transverse relaxation time (T_2) distribution calculated with the inverse Laplace transform for (a) L1, (b) L2, (c) L3, (d) L4 e (e) L5 leather specimens.

Table 7 Longitudinal relaxation time T_1 and the components of transverse relaxation time T_2 for L1–L5 leather specimens

Samples	T_1 (ms)	W_A (%)	T_{2A} (ms)	W_B (%)	T_{2B} (ms)	W_C (%)	T_{2C} (ms)	W_D (%)	T_{2D} (ms)
L1	36.6	74.3	0.22	16.8	0.86	8.80	19.26	—	—
L2	39.8	78.7	0.24	11.8	1.24	9.50	13.52	—	—
L3	38.7	71.5	0.27	10.3	2.21	18.20	22.13	—	—
L4	39.1	61.7	0.24	15.4	0.82	6.80	4.45	16.1	48.80
L5	43.7	68.0	0.23	13.8	0.55	6.90	3.32	11.3	48.80

time T_2 is more sensitive to the cross-linking degree of the matrix. The increase in T_1 agrees with the progressive increase of SAD5 content and leather thermal stability (T_{max}) decrease, as a direct relation between thermal stabilisation/destabilisation (*i.e.*, T_{max} increase/decrease) and T_1 decrease/increase has been reported.[55,68]

The transverse relaxation times T_2 of the investigated samples splits into three components: a short relaxation time (T_{2A}), in the range of (0.19–0.27) ms, attributable to the rigid/crystalline component of collagen matrix, a middle relaxation time (T_{2B}), in the range (0.54–2.27) ms, and a long relaxation time (T_{2C}), in the range (3.32–22.13) ms, both ascribable to the amorphous component.[62,72,73] The fact that T_{2A} does not vary significantly suggests that the re-tanning combination has little effect on the crystalline phase of collagen matrix. On the opposite, both T_{2B} and T_{2C} shown substantial variation: the higher values were measured for L1 and L2 and the lower for L4 and L5. The values obtained for L3 specimen are most likely influenced by the acrylic resin.[73] The higher values of T_{2B} and T_{2C} are related to a reduced chain mobility and can be interpreted in terms of a tighter packing of collagen 3D matrix due to the bonds (*i.e.*, cross-linking) established with the synthetic re-tanning agent. When the synthetic re-tanning agent and then tara were eliminated from the re-tanning combination, the chain mobility increased, with the consequent decrease of T_{2B} and T_{2C}. These results are in excellent agreement with those obtained by micro-DSC. The fourth long component T_{2D}, present in L4 and L5 specimens, is not well defined. It might be related to a possible interaction between a liquid phase and not interacted SAD5 molecules, namely those too large to penetrate the leather pores and remains attached to the surface of the leather.[74]

The spectral features of L1–L5 specimens were identified by ATR-FTIR spectroscopy. The spectra of all leather specimens displayed similar absorption bands in the range (1800–800) cm^{-1} (Fig. S9†). Amide I, amide II and amide III bands of collagen were found at 1659, 1555, 1235 cm^{-1}, respectively, while the absorptions specific to the carbohydrate moieties, ν(C–O) and ν(C–O–C), were visible at 1034 and 1081 cm^{-1}.[75,76] The increase in the intensity of the band at 1034 cm^{-1} is attributable to both SAD5 and synthetic re-tanning agent.[77,78] The intensity decrease of the band at 1397 cm^{-1}, corresponding to the vibrations of the primary alcohol group (–OH),[76] is most likely due to H-bond formation. Furthermore, the increase of the slight signal found at 1202 cm^{-1} in raw hide, and usually attributed to the stretching vibrations of the amide bonds (C–N) and the bending of the plane (N–H), could be related to the collagen-tara interaction, as a result of merging of the tara typical band at 1195 cm^{-1} with raw hide amide vibration.[79] In fact, in the L5 spectrum, this band becomes very weak again as tara was substituted by SAD5.

L1–L5 leather specimens were also compared in terms of mechanical resistance, vapour permeability, light fastness to artificial ageing and colour performance. Based on these performance parameters, the potential application of a new leather specimen is decided. In particular, good mechanical performance properties are expected from shoes, which carries the body weight while should ensure comfort and health. Water vapour permeability impacts key functional properties such as the breathability and the comfort of leather products. With growing stringent requirements for sports footwear, water vapour permeability is a critical characteristic of high-quality leather. Colour is a key-quality due to its visual impact and aesthetic value. White leather is the most challenging material to acquire. White is associated with concepts of cleanliness and positivity, which contributes to its popularity in the fashion industry. It is also notable for allow minimal pigment without other unwanted effects. The light fastness of leather describes its colour resistance to fading by light, in particular by the constant radiation of UV light. On the other hand, colour change due to modifications in leather processing has great importance, and to reproduce an exact desired colour every time, manufacturers and designers need ways to quantify colour's properties and determine the numerical difference between colours. For instance, colour lightness is critical for leathers could be dyed in bright colours.[11]

The suitability and the performance of the new leather specimens obtained using SAD5 as an eco-friendly re-tanning agent, according to the official test methods used in the tanning industry, is confirmed by the results listed in Table 8. It is worth mentioning that tanning agents are primarily used to enhance the thermal stability of leather, while re-tanning agents are essential for improving the final quality as well as the physical and sensory properties of the leather. One downside of replacing hydrocarbon-based synthetic products is that it can lead to a lower denaturation temperature. Although L4 may be suitable for applications in the automotive and design industries, L5 provides optimal characteristics for leather goods and fashion items. To ensure that the leather is marketable, the final shrinkage temperature, which is determined by the synergy of the tanning and re-tanning agents, must exceed 65 °C. Tensile strength and tear load are two distinct properties that help assess the durability and quality of leathers. Tear strength measures a leather's resistance to tearing or propagating a rip, while tensile strength evaluates its ability to withstand pulling or stretching forces. Leathers with high tensile strength are desired in applications where resistance to elongation and stretching is crucial, such as seatbelts, industrial safety harnesses, while leathers with better resistance to tearing are suitable for applications that involve frequent stress, such as sportswear. The wet white tanning process results in pure, intense, bright white colour when leather come out of the drum, which makes it perfectly adapted base for intense colours or bright pastels. The results in Table 8 confirm that L5 specimen (where all other re-tanning agents were replaced by SAD5) displays enhanced tear load, distension of grain, surface strength, light fastness and perceptual lightness of colour compared to the initial L1 specimen obtained using a combination of three commercial products, while only a slight decrease was observed for tensile strength and water vapour permeability. Lastly, the L5 specimen has a natural soft touch comparable to wet-white leathers already on the market.

Table 8 L1–L5 leather specimens features according to official standard tests used in the tanning industry

Property	L1	L2	L3	L4	L5	Method
$T_s{}^a$, °C	78.5 ± 0.2	78.5 ± 0.2	73.5 ± 0.2	70.5 ± 0.2	68.4 ± 0.2	ISO 3380 : 2015
Tensile strenght[b], %	32.4 ± 1.4	29.1 ± 1.2	11.5 ± 1.5	26.5 ± 1.5	28.4 ± 1.3	ISO 3376 : 2020
Tear load[c], N mm^{-1}	166.5 ± 1.5	151.0 ± 1.1	140.1 ± 1.5	128.9 ± 1.2	211.1 ± 1.5	ISO 3377–2 : 2016
Distension of grain[d], mm	9.3 ± 0.1	9.6 ± 0.1	10.7 ± 0.2	13.3 ± 0.1	10.4 ± 0.1	ISO 3379 : 2015
Surface strenght[d], Kg	65.9 ± 1.0	65.1 ± 1.5	28.3 ± 1.2	76.0 ± 1.5	67.1 ± 1.2	ISO 3379 : 2015
Vapour permeability[e], mg h^{-1} cm^2	10.6 ± 0.1	10.6 ± 0.1	10.3 ± 0.1	10.3 ± 0.1	9.3 ± 0.1	ISO 14268 : 2023
Light fastness[f], blue scale	3	2–3	2	2	3	ISO 105-B02:2014
Perceptual lightness of colour[g], %	100	114.34	231.97	342.99	326.03	ISO 11664-4:2008(E)/ CIE S 014-4/E:2007

[a] ISO 3380:2015 T_s = Shrinkage temperature: **https://www.iso.org/standard/61792.html**. [b] ISO 3376:2020 tensile strength that a specified load and elongation at maximum force of leather. **https://www.iso.org/standard/75173.html**. [c] ISO 3377-2:2016 specifies a method for determining the tear strength of leather using a double-edged tear. **https://www.iso.org/standard/68861.html**. [d] ISO 3379:2015 specifies a test method for the determination of distension and strength of the leather grain or finished surface. **https://www.iso.org/standard/63871.html**. [e] ISO 14268:2023 describes a method for determining the water vapour permeability of leather. **https://www.iso.org/standard/81968.html**. [f] ISO 105-B02:2014 specifies a method for determining the effect on the color due to the action of an artificial light source representative of natural daylight (D65). **https://www.iso.org/standard/65209.html**. [g] CIE Standard defines procedures for calculating the coordinates of the CIE 1976 L*a*b* (CIELAB) colour space and the Euclidean colour difference values based on these coordinates.

Parallelly, a study has been conducted by some of us to compare the chemical (substances soluble in dichloromethane, water and volatiles content, extractable organic and inorganic matter, ash and insoluble mineral matter, nitrogen and leather substance, total metal and formaldehyde content) and physical-mechanical properties (including surface burst, dry and wet flex resistance, rub fastness, accelerated aging color change and finishing adhesion) of the alginate-tanned leathers (mixed tara-SAD5-tanned leather L4, and SAD5-tanned leather L5) with those of both conventional leather (chromium- and aldehyde-tanned leather) and commercial alternative materials such as leatherette, Piñatex®, and Desserto®.[80] The reported results confirmed that alginate-tanned leathers meet the quality standards required for high-end footwear and leather goods. In particular, water resistance, durability, and wear performance were improved. It is important to note that the white leather, such as the L5 white specimen, is even more appreciated for its clean, elegant, and sophisticated appearance.

In the same study are reported the results of a laboratory test on the composting potential of alginate-tanned leather compared with chrome-tanned, vegetable-tanned and alternative synthetic materials.[80]

In fact, biodegradability is a vital indicator for assessing the sustainability of leather. It is well established that chrome-free tanned leather exhibits a higher degree of biodegradation and a faster degradation rate compared to chrome tanned leather. Notably, leathers tanned with biomass-based agents biodegrade even more readily, as the crosslinking network of biomass-tanned leather is more susceptible to microbial attack. Furthermore, thermal stability, regarded as a key indicator of tanning quality, has been found to be negatively correlated with the biodegradability of leather.[81] Alginate-tanned leather completely degraded after 21 to 25 days and conventional chrome-tanned leather after 35 days, while vegetable-tanned leather shown initial degradation at 60 days, and alternative synthetic materials did not start degrade even after 90 days. Alginate-tanned leather composts had lower levels of

Kjeldahl and ammoniacal nitrogen, suggesting a more efficient degradation and less nitrogen release. Consequently, our SAD-tanned leathers could also present a good compromise between biodegradability and tanning effects to mitigate the environmental effects of footwear waste. Over 24 billion pairs of shoes are produced globally each year and billions of shoes end up in landfills each year worldwide according to the World Footwear Year Book 2024.[82] The use of biodegradable re-tanning agents derived from renewable biomass by eco-friendly ultrasound-assisted processes without requiring significant modifications to technology creates a complex interplay between established practice and evolving expectations for sustainability. Moreover, the development of eco-friendly re-tanning agents is closely linked to the principles of circular economy which seeks to minimize waste and maximize resource efficiency. It involves not only finding alternatives to synthetic and potentially harmful chemicals but also increasing the possibilities to revalorize leather solid wastes, reducing the environmental footprint of the entire supply chain.

Experimental

Materials and methods

Industrial sodium alginate food grade (E401) was purchased from Brenntag S.P.A. and used without further purification. The sodium alginate (SA) solution (2% w/w) was obtained by mixing distilled water and sodium alginate under stirring for 12 hours to obtain a very homogeneous solution.

The calf hides used for the tanning tests at laboratory and micro-pilot scale were made available by the Leather and Footwear Research Institute (ICPI) of the National Research and Development Institute for Textiles and Leather (INCDTP), Bucharest. All other reagents required for the tanning tests were purchased from CHIMREACTIVE S.R.L. Tests were performed using a rotator drive stirrer unit STR4/4 (Bibby Scientific Ltd) set for continuous operation at 35 rpm to simu-

late the movement of the tanning drum. The raw hide was initially pre-treated with water and NaCl to fully hydrate, reaching a pH of 6.0 ± 0.5. In each vessel containing the SAD1–SAD10 solution (20 g) and NaCl (0.12 g), we added the pre-treated hide (0.5 g). The hides were stirred in the tanning float for 6 hours and left in the float overnight. The second day, the hides were stirred for other 6 h and left in the tanning float for a second night to optimize SAD penetration and bonding. Finally, the hides were washed and left to dry in air at room temperature.

Calf hides, reagents, and chemicals used for the tanning process at the industrial pilot scale were made available by A3 Leather Innovation Center from University of Lleida, Spain. The tanning test procedures are reported in the ESI (Tables S1–S5†).

Three types of US equipment (Fig. S1†) were used to treat the SA solution at atmospheric pressure and constant temperature (40 °C): a horn type transducer with a 13 mm titanium probe (Sonic Vibracell VCX 750), a bath type with a 5 cm titanium transducer (*multifrequency* transducer from *Meinhardt* Ultrasonics – 580; 864 and 1146 kHz) and a modified closed loop dual-frequency reactor (DFR) (Advanced Sonic Processing System, Oxford, CT, USA) with a 10 cm titanium probe and the two magnetostrictive transducers located 7.5 cm apart. The ultrasound frequencies of DFR are 16 and 20 kHz, and the maximum power of the two generators is approximately 600 W.[83] To maintain the reaction temperature, all US equipment was equipped with cooling liquid recirculation systems.

Viscosity was measured using a Brookfield Ametek DV2T viscometer using different cylindrical spindles depending on the viscosity of the sample. The shear-rate viscosity dependence was measured at $T = 20$ °C in the shear-rate range $(0.1–1000)$ s^{-1}.

GPC analyses were carried out using Water alliance e2695 instrument with four Ultrahydrogel 7.8 × 300 mm columns in series (1000–500–250–120) and a *refractive index detector* 2414 RI, using NaOH 0.1 M–NaNO$_3$ 0.1 M in ultrapure H$_2$O (pH 10.8) as eluent. The molecular weight was detected using pullulans as standard (range 739 000 ÷ 342 Da). The measures were carried out in the following setting: 0.700 mL min^{-1} flux, 80–90 bar, 40 °C and sample concentration of 0.3% wt in ultrapure H$_2$O (volume of injection 10 μL).[84,85]

^{1}H NMR spectra were recorded on a Bruker Avance-600 MHz [600 (^{1}H)] at 353 K using condition reported by Jensen.[52] Chemical shifts are reported relative to the residual solvent peak.

Infrared spectroscopy in attenuated total reflection mode (FTIR-ATR) analyses were carried out with an ALPHA spectrometer (Bruker Optics) equipped with a Platinum ATR module. The penetration depth, depending on the refractive indices of ATR crystal and sample, typically amounts to a few microns (*ca.* 0.5–3 μm). Spectra were recorded in the 4000–400 cm^{-1} spectral range with a 4 cm^{-1} resolution, using 32 scans. Opus software (Bruker Optics) was used for the acquisition and processing of spectra.

Thermogravimetric analysis was carried out with a TGA Q500 thermobalance (TA Instruments). The TG profiles were recorded in the temperature range (25–800) °C, at 10 °C min^{-1} heating rate, under 100 cm^3 min^{-1} air flow, using open plati-

num pans loaded with samples of about 7 mg. The balance resolution is 1 μg.

Micro-differential scanning calorimetry (micro-DSC) was carried out with a high-sensitivity Micro-DSC III calorimeter (SETARAM) and was performed in the temperature range (25–95) °C, at 0.5 °C min^{-1} heating rate, using 850 μl Hastelloy C cells. Samples of max. 10 mg were suspended in 0.5 M acetate buffer (pH = 5.0) directly in the measure cell and left for 30 minutes to fully hydrate before performing the measure. Experimental DSC data acquired with the SETARAM SetSoft2000 software were processed using PeakFit 4.1 (Jandel Scientific). DSC multiple peaks of the investigated samples were deconvoluted using the PeakFit asymmetric Gaussian fit function to improve the fit of the asymmetry in the peaks. Each reported value represents an average of three tests on fresh samples. Certified reference materials such as naphthalene, benzoic acid and gallium were used to check the supplier calibration constants in the working temperature region. Several melting runs performed under the same experimental conditions as those performed for hide and leather samples showed an agreement with the IUPAC recommended values of 0.05% for temperature and 0.25% for enthalpy.

Unilateral nuclear magnetic resonance measurements of relaxation times were performed with a NMR-MOUSE instrument (Bruker Biospin) interfaced with a single-sided sensor by RWTH Aachen University, operating at 13.62 MHz. The longitudinal relaxation time T_1 was measured with the Saturation Recovery pulse sequence followed by a CPMG-train in the detection period to increase the sensitivity, while the CPMG sequence (1024 echoes were recorded with an echo time 2τ of 84 μs at a depth of 3 mm) was used to measure the transverse relaxation time T_2, as previously reported.[22] The error in the reported T_1 and T_2 values is within 10% of the nominal values.

The shrinkage temperature of leather samples was measured with a Giuliani Shrinkage T_g tester IG/TG, according to the standard method ISO 3380:2015 [IULTCS/IUP 16]. The temperature measuring device is graduated to 1 °C and shown to be accurate to ±0.5 °C. The detection precision and reproducibility depend on the analyst's visual sensitivity, yet accuracy is sufficient for tanners' needs. Each reported value represents an average of three tests per sample. The standard deviation was less than 2 °C for all samples.

Physical-mechanical tests were performed according to the specific standard tests used in the tanning industry: tensile strength [IUP-6/EN ISO 3376], tear load [IUP-8/EN ISO 3377-2], distention [IUP-9/ISO 3379], surface strength [IUP-9/ISO 3379] and water vapour [IUP-15/EN ISO 14268].

Light fastness to artificial light was determined following the IUF-402/EN ISO105-B02 method while the colour was evaluated using a Datacolor spectrophotometer and the CIE 1976 L*a*b* colour space.

Conclusions

In this study, ten eco-friendly sodium alginate derivatives (SADs) were obtained by ultrasonic processing with various

ultrasonic equipment and varying the process parameters (US frequency, US intensity, and treatment time). The main aim of the ultrasonic depolymerisation of sodium alginate was to develop an efficient, simple, fast and cost-effective approach for obtaining custom-length alginate chains able to interact with collagen and hence, with potential use in the tannery sector. SADs were characterized by viscosimetric analysis, GPC analyses, ^{1}H NMR spectroscopy, thermal gravimetry and ATR-FTIR spectroscopy. Our findings confirmed that, in addition to the general benefits (lower energy consumption compared to traditional methods, shorter processing time, mild temperature conditions), ultrasonic technology provides additional benefits for the sodium alginate depolymerization process, such as better control over polymer size and distribution through the selection of the transducer type and process parameters (frequency and treatment time), as well as scalability. Furthermore, no harsh chemicals are required to cleave the polymer chains, such as hydrogen peroxide, periodate, or metal catalysts. The increased efficiency, selectivity, and control over sodium alginate depolymerization indicate that ultrasound technology is a valuable tool for an ecologically safe and energy-efficient industrial process.

SADś interaction with collagen was assessed using micro-DSC. The SAD showing the highest ability to interact with collagen in the hide matrix was selected to be tested as a wet white re-tanning agent at pilot scale. Five re-tanning combinations, including increasing SAD concentrations (*i.e.*, from 0 to 32%) were used to obtain five leather specimens which were characterized by both physical–chemical methods (micro-DSC, single-sided NMR, ATR-FTIR) and standard methods currently used in the tannery industry. Although the use of SAD slightly diminishes the thermal stability of leather, it increases leather biodegradability, which can be accepted as the price paid for mitigating the environmental effects of leather solid wastes. Notably, all other critical parameters, such as mechanical resistance, water vapour permeability, colour light fastness, and brightness, indicate that the specimen re-tanned with SAD only has the required performance for high-end leather products. The white leather's versatility in design, coupled with associations of luxury and purity, positions it as a premium material in various industries, including fashion, automotive design, and furniture. Its timeless appeal makes it a popular choice for high-end products. Although there are challenges related to maintenance and staining, the aesthetic appeal and symbolic associations of white leather ensure its enduring popularity. Further, several advantages of white leather that don't require dyes include less processing (which means less energy and waste production), hypoallergenicity (eliminates the possibility of skin irritation from dyes), durability and natural strength (guaranteed by the original integrity of the leather fibres), less fading over time compared to dyed leather, and environmental benefits (avoids the use of synthetic dyes, reduces water and chemical pollution). SAD and tara tannin re-tanning combination resulted in a good-quality leather, too. The use of the novel alginate-based re-tanning agents involves

not only the manufacture (re-tanning process), but also the disposal phase (solid waste recovery and leather goods re-utilization/recycling). In conclusion, the eco-friendly interplay of ultrasound technology combined with eco-friendly practices such as the use of a renewable bioresources, *i.e.*, alginate, and full replacement of fossil-based re-tanning agents, has a real potential to pave the way for enhancing the eco-efficiency of the manufacturing sector in particular and of the leather goods in general. However, implementing alginate-based tanning agents in industrial leather production presents several challenges, including cost, resource availability, scalability, and market acceptance. Although alginate is a bio-based material, it may be more expensive than traditional tannins like chromium salts. The commercial viability of alginate-based tanning may also be limited by the availability of resources, particularly if seaweed production cannot meet high demand. While lab-scale and pilot-scale results show promising performance, scaling up for industrial production could encounter obstacles in ensuring both efficiency and consistency from batch to batch. A rigorous assessment of these factors is essential for maintaining quality on a larger scale. Moreover, successful market adoption will require acceptance from manufacturers, brands, and consumers. Despite the growing interest in sustainable materials, the widespread adoption of alginate-tanned leather will depend on its ability to compete with traditional tanning methods in terms of cost and durability.

Author contributions

Data availability

The data supporting this article have been included as part of the ESI.†

Conflicts of interest

There are no conflicts to declare.

Acknowledgements

References

1 Europe Tannin Market Size, Share, Value, & Developments, https://www.databridgemarketresearch.com/reports/europe-tannin-market, (accessed January 7, 2025).

2 R. Ashraf, Top 10 Largest Leather Producing Countries Worldwide in 2023, https://blackbirdleathers.com/top-10-largest-leather-producing-countries-worldwide-in-2023/, (accessed April 6, 2025).

3 M. M. Hassan, J. Harris, J. J. C. Busfield and E. Bilotti, *Green Chem.*, 2023, **25**, 7441–7469.

4 A. D. Covington and W. R. Wise, *Tanning Chemistry: The Science of Leather*, The Royal Society of Chemistry, 2nd edn, 2019, pp. 409–433.

5 F. Pan, Y. Xiao, L. Zhang, J. Zhou, C. Wang and W. Lin, *J. Cleaner Prod.*, 2023, **383**, 135492.

6 W. Huang, Y. Song, Y. Yu, Y. Wang and B. Shi, *J. Leather Sci. Eng.*, 2020, **2**, 8.

7 X. Sun, Y. Jin, S. Lai, J. Pan, W. Du and L. Shi, *J. Cleaner Prod.*, 2018, **175**, 199–206.

8 R. Zhou, Y. Jin, S. Lai, L. Shi, L. Bai and Z. Peng, *J. Cleaner Prod.*, 2022, **339**, 130666.

9 Z. Tian, J. Ma, Q. Liu and H. Zhang, *React. Chem. Eng.*, 2023, **8**, 645–655.

10 Q. D. Yao, L. Wang, Y. X. Liang, H. T. Wen, Z. Niu, J. Chen and W. H. Dan, *Mater. Sci. Forum*, 2020, **996**, 48–55.

11 M. Sathish, B. Madhan and J. Raghava Rao, *Waste Manage.*, 2019, **87**, 357–367.

12 P. Puhazhselvan, A. Pandi, P. B. Sujiritha, G. S. Antony, S. N. Jaisankar, N. Ayyadurai, P. Saravanan and N. R. Kamini, *Process Saf. Environ. Prot.*, 2022, **157**, 59–67.

13 K. R. Ramya, M. Sathish, B. Madhan, S. N. Jaisankar and P. Saravanan, *J. Environ. Manage.*, 2022, **302**, 114029.

14 Discover the ECO Tanning – QUIMSER S.A. leather chemicals, https://quimser.com/eco-tanning/, (accessed April 18, 2025).

15 Communication from the Commission, https://oceans-and-fisheries.ec.europa.eu/publications/communication-commission-towards-strong-and-sustainable-eu-algae-sector_en, (accessed November 11, 2024).

16 România aruncă la gunoi algele marine, resursă regenerabilă importantă, deși UE recomandă folosirea lor | adevarul.ro, https://adevarul.ro/stiri-locale/constanta/romania-arunca-la-gunoi-algele-marine-resursa-2247963.html, (accessed November 11, 2024).

17 Y. Yu, Y. Lin, Y. Zeng, Y. Wang, W. Zhang, J. Zhou and B. Shi, *ACS Sustainable Chem. Eng.*, 2021, **9**, 6720–6731.

18 M. Nasrollahzadeh, N. Shafiei, Z. Nezafat, N. S. Soheili Bidgoli and F. Soleimani, *Carbohydr. Polym.*, 2020, **241**, 116353.

19 M. Crudu, M. C. E. Badea and C. Șendrea, *Miu*, RO135321A2, 2021.

20 W. Ding, J. Zhou, Y. Zeng, Y. Wang and B. Shi, *Carbohydr. Polym.*, 2017, **157**, 1650–1656.

21 W. Ding, Y. Yi, Y. Wang, J. Zhou and B. Shi, *ChemistrySelect*, 2018, **3**, 12330–12335.

22 I. Quaratesi, M. C. Micu, E. Rebba, C. Carsote, N. Proietti, V. Di Tullio, R. Porcaro and E. Badea, *Polymers*, 2023, **15**, 4676.

23 I. Quaratesi, I. Călinescu, P. Chipurici, E.-G. Dumbravă, A. Cucos, M. Y. Zaki, P. La Manna, A. Bercea, M. S. Stan, S. Michalik, C. Pearce, M. Odlyha, G. Burca and E. Badea, *J. Mol. Struct.*, 2025, **1328**, 141299.

24 L. Feng, Y. Cao, D. Xu, S. Wang and J. Zhang, *Ultrason. Sonochem.*, 2017, **34**, 609–615.

25 A. Dodero, S. Vicini and M. Castellano, *Food Hydrocolloids*, 2020, **109**, 106128.

26 T. J. Mason and M. Vinatoru, *Sonochemistry: applications and developments*, De Gruyter, Boston, 1. Auflage, 2022.

27 M. A. Moktadir, H. B. Ahmadi, R. Sultana, F.-T. Zohra, J. J. H. Liou and J. Rezaei, *J. Cleaner Prod.*, 2020, **251**, 119737.

28 Registration Dossier - ECHA, https://echa.europa.eu/it/registration-dossier/-/registered-dossier/15527, (accessed December 7, 2022).

29 Sodium periodate|7790-28-5 supplier and manufacturer - BuyersGuideChem, https://www.buyersguidechem.com/chemical_supplier/Sodium_periodate, (accessed February 13, 2023).

30 Substance Information – ECHA, https://echa.europa.eu/it/substance-information/-/substanceinfo/100.029.270, (accessed May 4, 2023).

31 K. Yasui, *Acoustic Cavitation and Bubble Dynamics*, Springer International Publishing, Cham, 2018, pp. 1–35.

32 B. Thokchom, A. B. Pandit, P. Qiu, B. Park, J. Choi and J. Khim, *Ultrason. Sonochem.*, 2015, **27**, 210–234.

33 J. Capelo, M. Galesio, G. Felisberto, C. Vaz and J. Pessoa, *Talanta*, 2005, **66**, 1272–1280.

34 M. Vinatoru and T. Mason, *Ultrason. Sonochem.*, 2017, **39**, 240–242.

35 J. Wang, Z. Wang, C. L. Z. Vieira, J. M. Wolfson, G. Pingtian and S. Huang, *Ultrason. Sonochem.*, 2019, **55**, 273–278.

36 S. Vajnhandl and A. Majcen Le Marechal, *Dyes Pigm.*, 2005, **65**, 89–101.

37 P. R. Gogate and A. L. Prajapat, *Ultrason. Sonochem.*, 2015, **27**, 480–494.

38 A. R. S. Santha Kumar, A. Padmakumar, U. Kalita, S. Samanta, A. Baral, N. K. Singha, M. Ashokkumar and G. G. Qiao, *Prog. Mater. Sci.*, 2023, **136**, 101113.

39 A. S. Kawadkar and P. R. Gogate, *Chem. Eng. Process.*, 2023, **191**, 109446.

40 A. Rasyid, *Oseana*, 2003, **28**, 33–38.

41 N. Devina, Y. K. Eriwati and A. S. Santosa, *Journal of Physics: Conference Series*, IOP Publishing, 2018, vol. 1073, pp. 052012.

42 V. S. Sutkar, P. R. Gogate and L. Csoka, *Chem. Eng. J.*, 2010, **158**, 290–295.

43 X. Bu and M. Alheshibri, *Ultrason. Sonochem.*, 2021, **76**, 105629.

44 S. S. Rashwan, I. Dincer and A. Mohany, *Ultrason. Sonochem.*, 2020, **68**, 105174.

45 S. M. H. Hosseini, Z. Emam-Djomeh, S. H. Razavi, A. A. Moosavi-Movahedi, A. A. Saboury, M. S. Atri and P. Van der Meeren, *Food Hydrocolloids*, 2013, **32**, 235–244.

46 K. V. B. Tran, Y. Asakura and S. Koda, *Jpn. J. Appl. Phys.*, 2012, **51**, 07GD06.

47 H. Lee and H. Feng, in *Ultrasound Technologies for Food and Bioprocessing*, ed. H. Feng, G. Barbosa-Canovas and J. Weiss, Springer New York, New York, NY, 2011, pp. 559–582.

48 F. J. O. Landa, S. R. Penacoba, F. M. de Espinosa, D. Razansky and X. L. Deán-Ben, *Ultrasonics*, 2019, **94**, 117–123.

49 A. Shrivastava, *Introduction to Plastics Engineering*, Elsevier, 2018, pp. 17–48.

50 I. Donati and B. E. Christensen, *Carbohydr. Polym.*, 2023, **321**, 121280.

51 C. Hu, W. Lu, A. Mata, K. Nishinari and Y. Fang, *Int. J. Biol. Macromol.*, 2021, **177**, 578–588.

52 H. M. Jensen, F. H. Larsen and S. B. Engelsen, in *Natural Products From Marine Algae*, ed. D. B. Stengel and S. Connan, Springer New York, New York, NY, 2015, vol. 1308, pp. 347–363.

53 T. M. Aida, T. Yamagata, M. Watanabe and R. L. Smith, *Carbohydr. Polym.*, 2010, **80**, 296–302.

54 H. Daemi and M. Barikani, *Sci. Iran.*, 2012, **19**, 2023–2028.

55 R. G. Huamani-Palomino, C. R. Jacinto, H. Alarcón, I. M. Mejía, R. C. López, D. D. O. Silva, E. T. G. Cavalheiro, T. Venâncio, J. Z. Dávalos and A. C. Valderrama, *Int. J. Biol. Macromol.*, 2019, **129**, 1056–1068.

56 B. Dupuy, A. Arien and A. P. Minnot, *Artif. Cells, Blood Substitutes, Biotechnol.*, 1994, **22**, 71–82.

57 D. Leal, B. Matsuhiro, M. Rossi and F. Caruso, *Carbohydr. Res.*, 2008, **343**, 308–316.

58 P. Rivero-Ramos, M. G. Unthank, T. Sanz, M. D. Rodrigo and M. Benlloch-Tinoco, *Carbohydr. Polym.*, 2023, **316**, 120999.

59 S. El Atouani, F. Bentiss, A. Reani, R. Zrid, Z. Belattmania, L. Pereira, A. Mortadi, O. Cherkaoui and B. Sabour, *Phycol. Res.*, 2016, **64**, 185–193.

60 I. H. Boyaci, H. T. Temiz, H. E. Geniş, E. Acar Soykut, N. N. Yazgan, B. Güven, R. S. Uysal, A. G. Bozkurt, K. İlaslan, O. Torun and F. C. Dudak Şeker, *RSC Adv.*, 2015, **5**, 56606–56624.

61 D. P. Valido, W. D. G. Júnior, M. E. De Andrade, A. A. Rezende, F. M. De Andrade De Carvalho, R. De Lima, G. Das Graças Gomes Trindade, C. De Alcântara Campos, A. M. S. Oliveira, E. P. B.S. S. De Souza, L. A. Frank, S. S. Guterres, E. M. Sussuchi, C. R. S. Matos, A. Polloni, A. A. De Souza Araújo, F. F. Padilha, P. Severino, E. B. Souto and R. L. C. De Albuquerque Júnior, *Drug Delivery Transl. Res.*, 2020, **10**, 1716–1728.

62 E. Badea, C. Şendrea, C. Carşote, A. Adams, B. Blümich and H. Iovu, *Microchem. J.*, 2016, **129**, 158–165.

63 C. Carsote and E. Badea, *Herit. Sci.*, 2019, **7**, 48.

64 P. G. Righetti and B. Verzola, *Electrophoresis*, 2001, **22**, 2359–2374.

65 P. L. Privalov and S. J. Gill, *Advances in Protein Chemistry*, Elsevier, 1988, vol. 39, pp. 191–234.

66 M. Roberge, R. N. A. H. Lewis, F. Shareck, R. Morosoli, D. Kluepfel, C. Dupont and R. N. McElhaney, *Proteins*, 2003, **50**, 341–354.

67 G. Bruylants, J. Wouters and C. Michaux, *CMC*, 2005, **12**, 2011–2020.

68 I. Quaratesi, I. Bruno, A. Pauciulo, A. R. Bartiromo, E. Badea, C. Carşote, P. Neri, C. Talotta, R. Gliubizzi, V. Di Tullio, N. Proietti, A. Cepparrone, F. Nuti, V. Ferrara and C. Gaeta, *Polym. Test.*, 2023, **129**, 108268.

69 M. Sathish, J. Raghava Rao and N. N. Fathima, *J. Appl. Polym. Sci.*, 2014, **131**, app.40835.

70 V. Sivakumar and P. G. Rao, *J. Cleaner Prod.*, 2001, **9**, 25–33.

71 C. Carsote, C. Şendrea, M.-C. Micu, A. Adams and E. Badea, *Radiat. Phys. Chem.*, 2021, **189**, 109712.

72 C. Sendrea, E. Badea and A. Adams, *Rev. Chim.*, 2017, **68**, 1780–1785.

73 C. Şendrea, C. Carsote, E. Badea, A. Adams, M. Niculescu and H. Iovu, *Sci. Bull. B Chem. Mater. Sci. UPB*, 2016, **78**, 27–38.

74 J. Wang, S. Lu, P. Zhang, Q. Li, Y. Yin, W. Li, N. Zhou, G. Chen, Y. Yi and C. Wu, *Fuel*, 2024, **374**, 132426.

75 K. Belbachir, R. Noreen, G. Gouspillou and C. Petibois, *Anal. Bioanal. Chem.*, 2009, **395**, 829–837.

76 T. Riaz, R. Zeeshan, F. Zarif, K. Ilyas, N. Muhammad, S. Z. Safi, A. Rahim, S. A. A. Rizvi and I. U. Rehman, *Appl. Spectrosc. Rev.*, 2018, **53**, 703–746.

77 T. Aguirre Calvo and P. Santagapita, *J. Qual. Reliab. Eng*, 2016, **2016**, 1–7.

78 A. Pragya, S. Mutalik, M. W. Younas, S.-K. Pang, P.-K. So, F. Wang, Z. Zheng and N. Noor, *RSC Adv.*, 2021, **11**, 10710–10726.

79 G. Tondi and A. Petutschnigg, *Ind. Crops Prod.*, 2015, **65**, 422–428.

80 N. P. Sardroudi, S. Sorolla, C. Casas and A. Bacardit, *Sustainability*, 2024, **16**, 2324.

81 Y. Wang, Y. Zhang and Z. Wang, *Collagen Leather*, 2024, **6**, 12.

82 W. Footwear, The World Footwear Yearbook 2024, **https://www.worldfootwear.com/news.asp?id=9952**, (accessed December 28, 2024).

83 I. Quaratesi, I. Calinescu, V. Lavric, V. Ferrara, E. Badea, P. Chipurici, E.-G. Dumbravă, R.-R. Constantinescu, N. D. Ignat and I. Popa, *Agronomy*, 2024, **14**, 1452.

84 B. Larsen, D. M. Salem, M. A. Sallam, M. M. Mishrikey and A. I. Beltagy, *Carbohydr. Res.*, 2003, **338**, 2325–2336.

85 S. X. Ci, T. H. Huynh, L. W. Louie, A. Yang, B. J. Beals, N. Ron, W.-G. Tsang, P. Soon-Shiong and N. P. Desai, *J. Chromatogr., A*, 1999, **864**, 199–210.